AIAA 81-4293

Boundary Condition Specification for Mobile Granular Propellant Bed Combustion Processes

D. Y. Chen,* V. Yang,* and K. K. Kuo†
The Pennsylvania State University, University Park, Pa.

In the modeling of transient one-dimensional, two-phase combustion of granular propellants in gun interior ballistics, the boundary conditions at both the breech end and the base of the projectile must be specified adequately. The form and the total number of the boundary conditions required depend upon the relative velocities of the gases and solid particles with respect to the solid boundary and the condition of fluidization. In the study of a simulated gun system, the flow properties at the boundary are obtained by considering 1) the local balances of mass, momentum, and energy over a small control volume adjacent to the boundary; 2) the compatibility relationships along the characteristic lines; and 3) the number of algebraic relationships according to the instantaneous flow conditions. These considerations are necessary to provide the extraneous boundary conditions required for solving the partial differential equations with a second-order numerical scheme. Numerical results were compared and found in agreement with test-firing data.

Nomenclature

A = cross-sectional area of cylindrical combustion chamber
A_s = specific surface area of granular propellants, the surface exposed to fluid per unit volume
C = speed of sound in particle phase
C_L = combustion chamber length
C_v = specific heat at constant volume
C_p = specific heat at constant pressure
dx/dt = slope of characteristic equations
D_p = drag force due to porosity gradient
D_t = total drag force between gas and particle phases, $D_t = D_v + D_p = D_v - (P/A_s)(\partial\phi/\partial x)$
D_v = drag force acting on gases by particles per unit wetted area of particles (evaluated from Kuo-Nydegger correlation)
D/Dt = Lagrangian time derivative when observer follows motion of the bullet, $(\partial/\partial t) + u_B(\partial/\partial x)$
E = total stored energy (internal plus kinetic energy) per unit mass
h_c = average convection heat-transfer coefficient over pellets
h_{chem} = enthalpy of propellant gas at flame temperature
h_{ign} = enthalpy of igniter gas
h_t = total heat transfer coefficient, the unit-surface conductance
k = thermal conductivity of gases
k_p = thermal conductivity of particles
K = coefficient of characteristic equations
M_{ign} = igniter mass flow rate
P = pressure
$\mathcal{P}_{wg}$ = wetter perimeter between chamber wall and gas phase
$\mathcal{P}_{wp}$ = wetter perimeter between chamber wall and particle phase
q = rate of conduction heat transfer per unit area
$\dot{Q}_w$ = rate of heat loss to chamber wall per unit spatial volume of gas-particle system
r_b = burning rate of solid propellant
r_p = radius of pellets
R = gas constant
t = time
T = temperature
T_{abl} = ablation temperature of solid propellant
T_f = adiabatic flame temperature of pellets
T_{hg} = temperature of hot igniter gas
T_{ps} = particle surface temperature
T_{ign} = ignition temperature of solid propellant
U = velocity with respect to laboratory coordinates
u_B = projectile velocity with respect to laboratory coordinates
Ug_{ign} = igniter gas velocity
x = distance from beginning of granular propellant bed
x_B = instantaneous location of base of projectile
x_L = left boundary of partial-differential-equation solution portion (interior region) of granular bed
$x_{\ell c}$ = length of left control volume
x_R = right boundary of partial-differential-equation solution portion of granular bed
x_{rc} = length of right control volume
α_p = thermal diffusivity of pellets
γ = specific heat ratio
Δ = difference
μ = dynamic viscosity of gas phase
ρ = gas density
ρ_p = density of pellets
τ_p = intergranular stress transmitted through solid propellants (τ_p = intragranular stress + P)
τ_{wg} = shear stress between chamber wall and gas phase
τ_{wp} = shear stress between chamber wall and particle phase
ϕ = fractional porosity
ϕ_c = critical porosity

Subscripts and Superscripts

g = gas phase
ℓc = evaluated at left control volume
p = particle phase
P = pressure
rc = evaluated at right control volume
tm = time
T = gas temperature
T_{ps} = particle surface temperature

Received Sept. 18, 1980; revision received March 12, 1981.

*Graduate Assistant.
†Professor. Associate Fellow AIAA.

U_g = gas velocity
U_p = particle velocity
ϕ = porosity
x_L = evaluated at left boundary
x_R = evaluated at right boundary
I,II = along right- and left-running characteristic line in gas phase, respectively
III = along gaseous-path characteristic line in gas phase
IV,V = along right- and left-running characteristic line in particle phase, respectively
VI = along particle-path characteristic line in particle phase
0 = initial state

I. Introduction

THE combustion of granular solid propellants in a mobile bed with a moving boundary (as in the case of gun interior ballistics) is highly transient and extremely complex. The theoretical modeling of the complicated flame spreading and combustion phenomena in granular beds is a challenge to engineers and scientists. In the last decade, progress on the theoretical modeling has been made by advancing from the lumped parameter analysis[1] to the fixed granular bed combustion[2] and to the mobile granular bed combustion models.[3-6] In the modeling of mobile granular bed combustion processes, several quasi-one-dimensional time-dependent combustion models have been independently developed[3-6] and reviewed.[7]

Additional modifications and improvements have been made recently in these models. The Pennsylvania State University model has been improved in the following areas: 1) the boundary condition treatment, especially the moving boundary at projectile end, was significantly improved (detailed approach and results are given in this paper and Ref. 8); 2) measurements and correlations of the intragranular stress and particle-wall friction in granular propellant beds were made[9]; 3) the speed of sound transmitted through a packed granular bed as a function of porosity was obtained[9]; 4) a primer characterization study was conducted to determine the actual flow rates from percussion primers (results of this study[10] were used as input data for granular bed combustion calculations); 5) the initial transient granular bed compaction caused by venting or primer products was studied[11]; and 6) the one-dimensional assumption used in the theoretical model was examined experimentally.[11]

In Gough's model, the boundary condition calculations have been improved[12,13] by considering two types of boundaries, one for a rigid, impermeable wall that is either stationary or mobile, and the other for a rigid, gas-permeable stationary wall. The first type is applied to the base of the projectile or to the breech of a gun; the second type is applied to recoilless rifles and high-low guns. Since Gough's main interest was in large caliber systems, special emphasis was placed on the description of the bags, plugs, wads, cardboard spacers, and other filler materials between the propellant and the projectile. He used a lumped parameter analysis coupled with compatibility conditions and isentropic relationships to compute the flow properties at both internal and external boundaries. Gough has recently developed a two-dimensional convective flame-spreading model for large caliber systems in which the multidimensional effect is important.[14] However, the two-dimensional effect is not important for small caliber systems[11] and therefore is not addressed in this paper.

In the study of deflagration-to-detonation transition (DDT) phenomena in granular propellant beds, Krier and Kezerle have changed the earlier continuum mechanics model[4] developed at the University of Illinois into a separated two-phase flow model.[15] A number of empirical correlations were altered for use beyond the ranges for which these correlations were developed. The lack of suitable constitutive relationships under DDT conditions were noted.

Although numerous papers and reports have been published on the combustion of granular propellants, information available on the treatment of the boundary conditions is limited. This lack of information is probably due to the fact that in the initial development of theoretical models most researchers emphasized the governing equations and the necessary empirical correlations required as physical input functions in the theoretical model. Since the boundary conditions used in the theoretical computations may alter results significantly, the objectives of this study are:

1) To illustrate the dependence of the number of boundary conditions on flow situations.

2) To specify the boundary conditions used for various flow conditions near the breech end and the projectile base of a simulated gun system.

3) To test the predictability of the theoretical model for mobile granular bed combustion processes by comparing theoretical results with experimental data.

II. Method of Approach

A. Experimental Setup and Measurements

The purpose of conducting an experimental investigation is to provide experimental data for theoretical model validation. The current experimental setup is quite similar to that used by Davis and Kuo.[16] Major differences between these two setups lie in the measurement technique of the projectile displacement and the event trigger system. To facilitate understanding of the experimental test rig used in this study, a brief description is given below (see Refs. 8 and 16 for more detailed information).

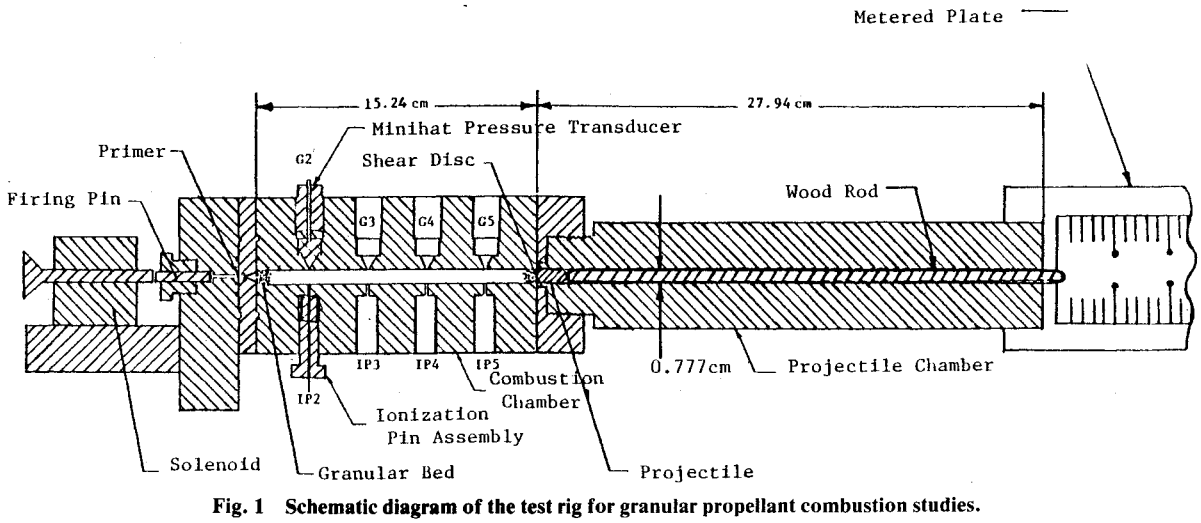

Fig. 1 Schematic diagram of the test rig for granular propellant combustion studies.

The granular bed experimental setup essentially consists of three components: a percussion primer unit, a thick-walled instrumented combustion chamber, and a barrel chamber, as shown in Fig. 1. The inner diameter of the combustion chamber is 0.777 cm, and the initial length of the combustion chamber is 15.24 cm. The chamber is sealed with a thin steel shear disk (0.0914 cm thick) which keeps the chamber sealed before the occurrence of disk rupture. A brass/lead projectile is installed in front of the shear disk. At the onset of disk rupture, the projectile begins to move. In order to detect the instantaneous projectile location, a wood stick (diameter = 0.64 cm) is placed directly in front of the projectile. The stick used in this study has an aerodynamically shaped head, and is long enough to protrude beyond the muzzle of barrel chamber; thus the motion of the projectile, as indicated by the motion of the wood stick against a stationary metered plate, can be filmed by a high-speed camera (400-ft capacity Hycam Model K20S4E-115) with framing rate around 22,000 pictures/s. The camera also serves as the triggering device for activating the solenoid armature and firing pin.

The purpose of measuring projectile displacement is not to compare the measured projectile velocity with the predicted value. Any projectile velocity prediction involves such uncertainties as frictional resistance between the projectile and the gun barrel, pressure distribution around the projectile, heat losses, etc. Uncertainties of this type are not desirable for model validation. The intent of this work is to compare the calculated pressure-time traces with the measured pressure-time traces. Recorded projectile displacement is used simply as input data for determining instantaneous combustion chamber length. Chamber length is considered as a known quantity in the numerical computation.

Besides having the capability for making projectile displacement measurements, the combustion chamber is instrumented with four pressure gages (Minihat resistance-type gages) and four ionization probes mounted along the granular bed on the side opposite the pressure gages. The ionization probes, mounted flush with the inner surface of the combustion chamber, are used to determine the arrival of the hot gas front. The experimental results obtained in primer characterization studies[10] are used as input data for primer mass and energy fluxes into the granular bed.

B. Theoretical Formulation of Boundary Conditions

Before considering the complicated two-phase combustion problem, it may be helpful to use a simpler example of a single-phase flow in a cylindrical tube to illustrate the dependence of the number of physical boundary conditions on flow situations. Let us consider a one-dimensional unsteady flow situation in which the drag and heat transfer between the gas and tube wall can be written in algebraic terms. The flow properties, such as gas temperature, pressure, and velocity, can be solved from a set of three coupled first-order partial differential equations (i.e., the conservation equations of mass, momentum, and energy). It is easy to see that this set of equations is hyperbolic in nature[2]; the eigenvalues are $-(U_g+C_g)$, $-(U_g-C_g)$, and $-U_g$. The slopes of the characteristic right-running and left-running waves and pathlines are:

$$\left(\frac{dx}{dt}\right)_{I}=U_g+C_g;\quad \left(\frac{dx}{dt}\right)_{II}=U_g-C_g;\ \text{and}\ \left(\frac{dx}{dt}\right)_{III}=U_g \quad (1)$$

In order to solve this set of first-order hyperbolic partial differential equations by using a second-order finite-difference approximation, three boundary conditions must be specified at each end of the tube. The boundary conditions can come either from physical conditions, or compatibility relationships obtained from the method of characteristics. Focusing attention on the left end of the tube, one should consider four different cases shown in Fig. 2.

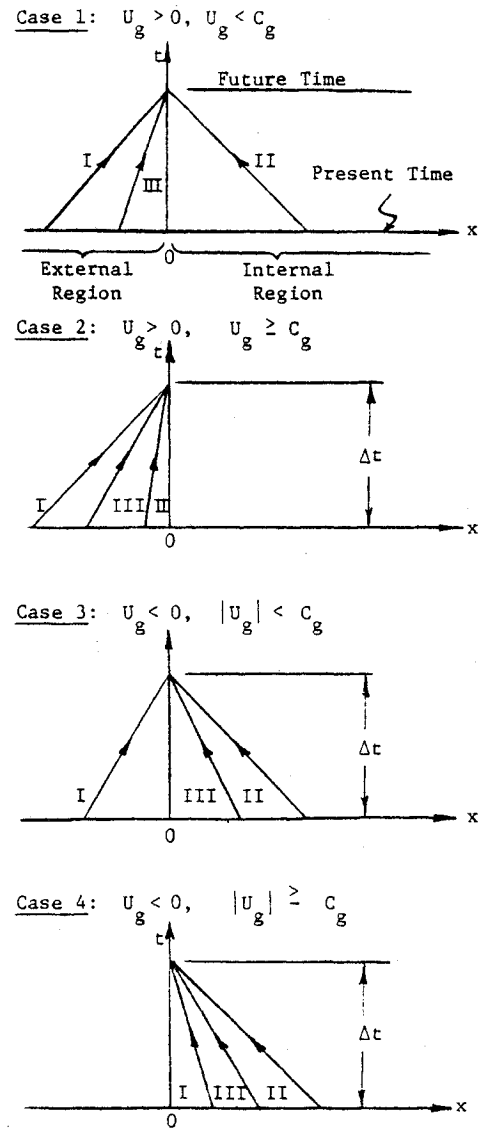

Fig. 2 The dependence of boundary condition specifications on flow situations (single-phase).

Case 1 represents a subsonic inflow of gas into the tube. The left-running characteristic line (II) can serve as a compatibility relationship at the tube opening; therefore, two physical boundary conditions must be specified. Case 2 represents a sonic or supersonic inflow of gas into the tube. Since there is no characteristic line running from the interior region at the present time level to the boundary point at the future time level, three physical boundary conditions should be specified. Case 3 represents a subsonic outflow of gas at the tube opening. Two characteristic lines (II and III) run from the interior region at the present time to the boundary point at the future time; therefore, only one physical boundary condition can be specified. Case 4 represents a sonic or supersonic outflow of gas at the tube opening. Since no outside disturbances can propagate to the inside of the tube, no physical boundary condition can be specified. The boundary conditions are determined solely from the compatibility relations along three characteristic lines.

From the above discussion, it is easy to see that the number of physical boundary conditions required depends not only upon the flow direction but also upon the relative magnitude of the gas velocity with respect to the speed of sound.

The boundary conditions for two-phase granular propellant combustion are much more complex than those for single-phase flows. Strictly speaking, the system of governing equations is not totally hyperbolic, but has some hyperbolic

features. In order to solve the partial differential equations more easily, the system can be arranged into a totally hyperbolic form by adding a drag term, D_p, on both sides of the gas-phase momentum equation and by treating this porosity gradient drag term as an inhomogeneous term. By so doing, the governing equations become totally hyperbolic in form with six real eigenvalues corresponding to six characteristic equations.[17] The slopes of the characteristic lines for the gas phase are the same as those given in Eq. (1). The slopes of the characteristic lines for the solid phase are:

$$\left(\frac{dx}{dt}\right)_{IV} = U_p + C; \quad \left(\frac{dx}{dt}\right)_{V} = U_p - C; \text{ and } \left(\frac{dx}{dt}\right)_{VI} = U_p \quad (2)$$

For nonfluidized granular beds, the speed of sound transmitted in the solid propellant aggregate is nonzero; the characteristic lines (IV, V, and VI) run in different directions. However, as soon as the granular bed becomes fluidized, C declines drastically and the three characteristic lines collapse nearly into one. Under this situation, the system of governing differential equations essentially changes from totally hyperbolic to hyperbolic. It is therefore not adequate to use all three solid-phase compatibility relations for numerical solutions.

The six characteristic equations (or compatibility conditions) are given below:

1) The right-running characteristic equation in the gas phase is

$$K^{I}_{U_g}(dU_g)_I + K^{I}_{P}(dP)_I + K^{I}_{U_p}(dU_P) + K^{I}_{\phi}(d\phi)_I = K^{I}_{tm}\Delta t \quad (3)$$

where $K^{I}_{U_g}$, K^{I}_{p}, etc., are coefficients for the characteristic line I. These coefficients are given in Ref. 17.

2) The left running characteristic equation in the gas phase is

$$K^{II}_{U_g}(dU_g)_{II} + K^{II}_{P}(dP)_{II} + K^{II}_{U_P}(dU_p)_{II} + K^{II}_{\phi}(d\phi)_{II} = K^{II}_{tm}\Delta t \quad (4)$$

3) The gas-phase path line characteristic equation is

$$K^{III}_{T}(dT)_{III} + K^{III}_{P}(dP)_{III} + K^{III}_{U_P}(dU_P)_{III} + K^{III}_{\phi}(d\phi)_{III} = K^{III}_{tm}\Delta t \quad (5)$$

4) The right-running characteristic equation in the particle phase is

$$K^{IV}_{U_P}(dU_P)_{IV} + K^{IV}_{\phi}(d\phi)_{IV} = K^{IV}_{tm}\Delta t \quad (6)$$

5) The left-running characteristic equation in the particle phase is

$$K^{V}_{U_P}(dU_P)_{V} + K^{V}_{\phi}(d\phi)_{V} = K^{V}_{tm}\Delta t \quad (7)$$

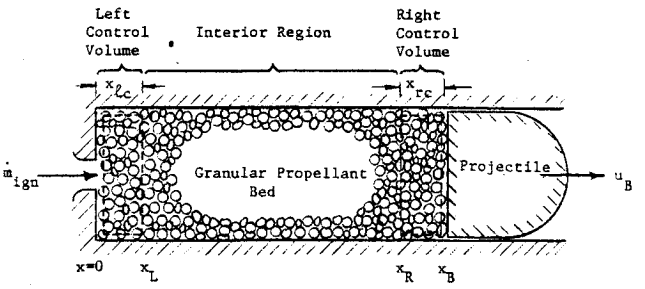

Fig. 3 The left and right control volumes of the granular propellant bed.

6) The particle-phase path line characteristic equation is

$$K^{VI}_{T_{ps}}(dT_{ps})_{VI} + K^{VI}_{T}(dT)_{VI} = K^{VI}_{tm}\Delta t \quad (8)$$

Mathematically, the above compatibility relationships can be used to link flow properties in the interior region of the granular bed to those at the boundary surfaces, viz., primer exit plane ($x=0$) and the base of the projectile or the inner surface of the shear disk ($x=x_B$). However, many complicated three-dimensional phenomena occur near the boundary surfaces. These processes include, for example, expansion processes of the primer jet entering the granular bed, local void volume generation, gas and particle recirculation, nonuniform heating of granular propellants by primer products, segregation of the moving projectile base from the granular bed, local vorticity generation near the base of the accelerating projectile, etc. These complicated processes cannot be adequately simulated by the quasi-one-dimensional model.

To bypass the complexities in the boundary regions, a lumped parameter analysis for the two regions is justified. At the projectile base, the right boundary is selected at x_R, which is located a short distance (x_{rc}) from the projectile base (see Fig. 3). The right control volume for the gas phase is the spatial volume between x_R and x_B minus the volume occupied by solid particles. The control volume considered for the particle phase is complementary to the gas-phase control volume. For the sake of simplicity, the spatial volume is defined as having a fixed width (x_{rc}) and moving along with the projectile. The flow properties in the small right control volume of the gas-phase are considered to be uniform. Similarly, the solid particles in the small control volume are considered to have uniform velocity and surface temperatures. These properties can be solved from the lumped parameter analysis described below.

The continuity equation for the gases inside the right control volume can be written as:

$$\frac{D(\rho\phi)_{rc}}{Dt} = \frac{(A\rho\phi)_{x_R}}{Ax_{rc}}[U_g(t,x_R) - u_B(t)] + (A_s\rho_p r_b)_{rc} \quad (9)$$

where D/Dt represents the Lagrangian derivative following the motion of the projectile.

The gas-phase momentum equation is:

$$\frac{D[\rho\phi(U_g-u_B)]_{rc}}{Dt} = \frac{(A\rho\phi)_{x_R}[U_g(t,x_R)-u_B(t)]^2}{Ax_{rc}} - \frac{(\tau_{wg}\mathcal{P}_{wg}x_{rc})_{rc}}{Ax_{rc}} + (A_s\rho_p r_b)_{rc}[U_p(t,x_{rc})-u_B(t)]$$
$$-(D_v A_s)_{rc} + \frac{1}{x_{rc}}[\phi(t,x_R)P(t,x_R) - \phi(t,x_B)P(t,x_B)] \quad (10)$$

The gas-phase energy equation is:

$$\frac{D[\rho\phi\{C_vT + \tfrac{1}{2}(U_g-u_B)^2\}]_{rc}}{Dt} = \frac{(A\rho\phi)_{x_R}[U_g(t,x_R)-u_B(t)][C_pT+\tfrac{1}{2}(U_g-u_B)^2]_{x_R}}{Ax_{rc}} - \frac{q(t,x_B)\phi(t,x_B)}{x_{rc}}$$
$$+\frac{q(t,x_R)\phi(t,x_R)}{x_{rc}} + (A_s\rho_p r_b)_{rc}\{h_{chem} + \tfrac{1}{2}[U_p(t,x_{rc})-u_B(t)]^2\} - \left(P\frac{d\phi}{dt}\right)_{rc} - (\dot{Q}_w)_{rc}$$
$$-[A_s(U_p-u_B)D_v]_{rc} - [A_s\bar{h}_t(T-T_{ps})]_{rc} \quad (11)$$

The particle-phase mass equation is:

$$\frac{D[\rho_p(1-\phi_{rc})]}{Dt} = -(A_s\rho_p r_b)_{rc} + \frac{\rho_p A[1-\phi(t,x_B)][U_p(t,x_R)-u_B(t)]}{Ax_{rc}} \tag{12}$$

The particle-phase momentum equation is:

$$\frac{D[\rho_p(1-\phi_{rc})(U_{p_{rc}}-u_B)]}{Dt} = (D_v A_s)_{rc} + \frac{\rho_p A(1-\phi_{x_R})[U_p(t,x_R)-u_B(t)]^2}{Ax_{rc}} - (A_s\rho_p r_b)_{rc}[U_{p_{rc}}-u_B(t)]$$

$$-\frac{(\tau_{wp}\mathcal{P}_{wp}x_{rc})_{rc}}{Ax_{rc}} - \frac{\tau_p(t,x_R)[1-\phi(t,x_R)]}{x_{rc}} + \frac{\tau_p(t,x_B)[1-\phi(t,x_B)]}{x_{rc}} \tag{13}$$

As with the right boundary, a left control volume is used for the breech end (see Fig. 3). The lumped parameter analysis for the left control volume consists of the following five ordinary differential equations.

The gas-phase mass equation is:

$$\frac{d(\phi\rho)_{\ell c}}{dt} = \frac{1}{Ax_{\ell c}}[\dot{m}_{ign_g}(t) - \rho(t,x_L)A\phi(t,x_L)U_g(t,x_L)] + (A_s r_b\rho_p)_{\ell c} \tag{14}$$

The gas-phase momentum equation is:

$$\frac{d(\rho U_g\phi)_{\ell c}}{dt} = \frac{1}{Ax_{\ell c}}(\dot{m}_{ign_g}(t)U_{g_{ign}} - \rho U_g^2 A\phi|_{x_L}) - \frac{(\tau_{wg}\mathcal{P}_{wg}x_{\ell c})_{\ell c}}{Ax_{\ell c}} + (A_s r_b\rho_p U_p)_{\ell c}$$

$$-(A_s D_v)_{\ell c} + \frac{1}{x_{\ell c}}[\phi(t,0)P(t,0) - \phi(t,x_L)P(t,x_L)] \tag{15}$$

The gas-phase energy equation is:

$$\frac{d(\rho\phi E)_{\ell c}}{dt} = (A_s\rho_p r_b)_{\ell c}\left(h_{chem} + \frac{U_p}{2}\right)_{\ell c} - (A_s D_v U_p)_{\ell c} - [A_s\bar{h}_t(T-T_{ps})]_{\ell c} + \frac{1}{Ax_{\ell c}}\left[\dot{m}_{ign_g}(t)\left(h_{ign} + \frac{U_{g_{ign}}^2}{2}\right)\right.$$

$$\left.-\rho U_g A\phi\left(C_p T + \frac{U_g^2}{2}\right)\Big|_{x_L}\right] - \frac{1}{x_{\ell c}}[q(t,x_L)\phi(t,x_L) + q(t,0)\phi(t,0)] - \left(P\frac{d\phi}{dt}\right)_{\ell c} - (\dot{Q}_w)_{\ell c} \tag{16}$$

The particle-phase mass equation is:

$$\frac{d[(1-\phi)\rho_p]_{\ell c}}{dt} = \frac{\dot{m}_{ign_p}(t)}{Ax_{\ell c}} - (A_s\rho_p r_b)_{\ell c} - \frac{\rho_p(1-\phi)U_p}{x_{\ell c}}\Big|_{x_L} \tag{17}$$

The particle-phase momentum equation is:

$$\frac{d[(1-\phi)\rho_p U_p]_{\ell c}}{dt} = -\frac{(1-\phi)\rho_p U_p^2}{x_{\ell c}}\Big|_{x_L} + (A_s D_v)_{\ell c} - (A_s r_b\rho_p U_p)_{\ell c} + \frac{1}{Ax_{\ell c}}\dot{m}_{ign_p}(t)U_{p_{ign}}$$

$$+\frac{\tau_p(t,x_L)[1-\phi(t,x_L)]}{x_{\ell c}} - \frac{\tau_p(t,0)[1-\phi(t,0)]}{x_{\ell c}} - \frac{(\tau_{wp}\mathcal{P}_{wp}x_L)_{\ell c}}{Ax_{\ell c}} \tag{18}$$

The physical boundary conditions required for solving this problem are mass and energy fluxes from the igniter system and projectile velocity. These enter directly into the inhomogeneous terms of the above lumped parameter analysis.

C. Numerical Treatment of Boundary Conditions

The total number of boundary conditions needed for solving the set of governing equations of transient two-phase flows in gun systems depends upon the flow directions of the gas and particles and on the fluidization conditions at the boundaries. For the case of mobile granular bed combustion with a moving boundary, there are eight possible cases for the left boundary conditions (LBC) and eight possible cases for the right boundary conditions (RBC). Each case designates a different combination of fluidization conditions at the boundary and relative magnitudes of the velocities. They are summarized as follows:

LBC
- $\phi \le \phi_c$ (nonfluidized)
  - $U_g \ge 0$
    - $U_p \ge 0$ ....LBC 1
    - $U_p < 0$ ....LBC 2
  - $U_g < 0$
    - $U_p \ge 0$ ....LBC 3
    - $U_p < 0$ ....LBC 4
- $\phi_c < \Phi < 1$ (fluidized)
  - $U_g \ge 0$
    - $U_p \ge 0$ ....LBC 5
    - $U_p < 0$ ....LBC 6
  - $U_g < 0$
    - $U_p \ge 0$ ....LBC 7
    - $U_p < 0$ ....LBC 8

$$
\text{RBC}\begin{cases}
\phi \le \Phi_c \text{ (nonfluidized)} \begin{cases} U_g \ge u_B \begin{cases} U_p \ge u_B \ldots\text{RBC 1} \\ U_p < u_B \ldots\text{RBC 2} \end{cases} \\ U_g < u_B \begin{cases} U_p \ge u_B \ldots\text{RBC 3} \\ U_p < u_B \ldots\text{RBC 4} \end{cases} \end{cases} \\
1 > \phi > \phi_c \text{ (fluidized)} \begin{cases} U_g \ge u_B \begin{cases} U_p \ge u_B \ldots\text{RBC 5} \\ U_p < u_B \ldots\text{RBC 6} \end{cases} \\ U_g < u_B \begin{cases} U_p \ge u_B \ldots\text{RBC 7} \\ U_p < u_B \ldots\text{RBC 8} \end{cases} \end{cases}
\end{cases}
$$

After solving for the lumped parameters in boundary control volumes and selecting the appropriate right and left boundary case, flow properties at boundaries can then be calculated from the extraneous boundary conditions and some algebraic relations based upon realistic assumptions. Detailed procedures for calculating flow properties at boundaries under all flow conditions are given in Ref. 8.

In terms of numerical schemes used, the sophisticated fourth-order Runge-Kutta integration method (RK4) was employed to solve the two sets of ordinary differential equations which govern flow properties in the left and right control volumes and, therefore, to determine lumped parameters inside control volumes. The same integration method was also used to carry out integration along characteristic lines. Iteration method was used to solve properties on the boundaries, lumped parameters in the boundary control volumes, and the axial locations of the intersections of the characteristic lines with the x axis. The modified two-step Richtmyer scheme[3] with predictor and corrector calculations was used in the interior region of the granular bed. The first step is a diffusing scheme which uses the central difference method in space and the forward difference method in time; the second step is a modified leap-frog scheme which also uses the central difference method in space and the forward difference method with double increments in time.

The expansion of the granular bed due to motion of the projectile was treated with a fixed number of nodes in the finite-difference calculation. After shot start, an interpolation method was used to determine the flow properties of the previous time levels at the expanded space location. The stretching of the mesh size in the x direction was uniform throughout the granular bed; at any given time, the mesh size was uniform throughout the interior region. For more detailed information, see Ref. 8.

Table 1 Computer program input variables

$T_0 = 293.91$ K	$r_{p_0} = 0.041275$ cm
$P_0 = 1$ atm	$\alpha_p = 0.945 \times 10^{-3}$ cm^2/s
$U_{g_0} = 0$ m/s	$\rho_p = 1.6$ g/cm^3
$U_{p_0} = 0$ m/s	$k_p = 0.53 \times 10^{-3}$ cal/cm-s-K
$\phi_0 = 0.4054$	$T_{abl} = 525$ K
$x_{tc} = 1.6815$ cm	$T_{ign} = 550$ K
$x_{rc} = 1.6815$ cm	$T_f = 2831$ K
$C_L = 15.24$ cm	

Table 2 Empirical correlations used in the theoretical model

Correlation	Reference
Intragranular stress	Kuo, Yang, and Moore[9]
Particle-wall friction	Kuo, Yang, and Moore[9]
Interphase drag	
Nonfluidized region	Kuo and Nydegger[18]
Fluidized region	Andersson[19]
Convective heat transfer	
Nonfluidized region	Denton[20]
Fluidized region	Rowe and Claxton[21]
Burning rate	Riefler and Lowery[22]

III. Discussion of Results

The Mobile Granular Bed Combustion (MGBC) computer program[8,17] was used to study MGBC processes with a moving projectile at the right boundary. Major input data and empirical correlations used to simulate a typical experimental test firing condition are given in Tables 1 and 2, respectively. In the experimental setup, a FA-34 primer was used to ignite 6.875 g of deterred WC-870 ball propellants. The initial porosity of the granular bed was 0.4054. Test chamber was

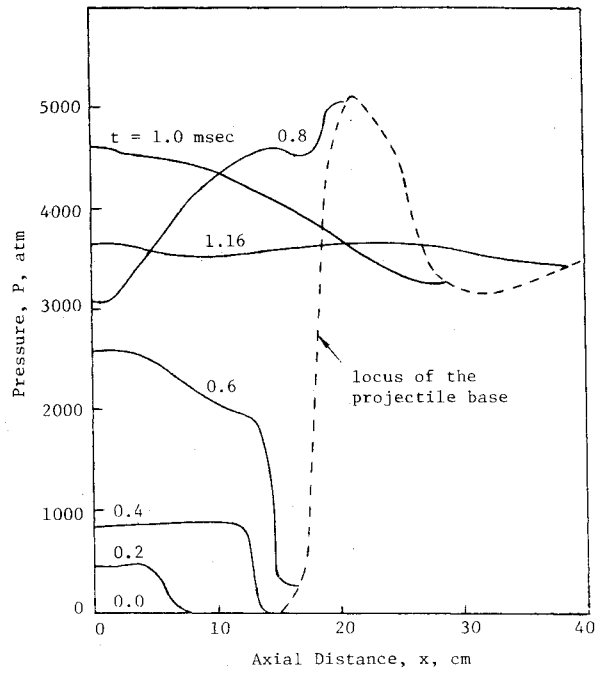

Fig. 4 Theoretically predicted pressure distributions at various times.

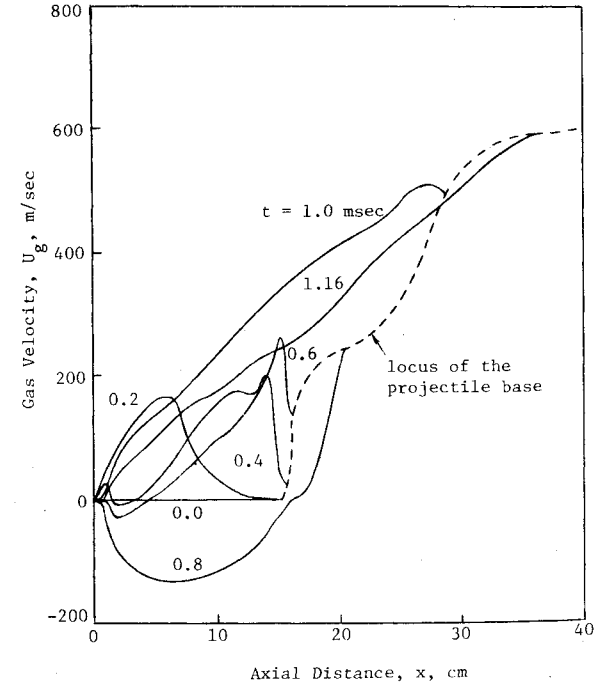

Fig. 5 Theoretically predicted gas velocity distributions at various times.

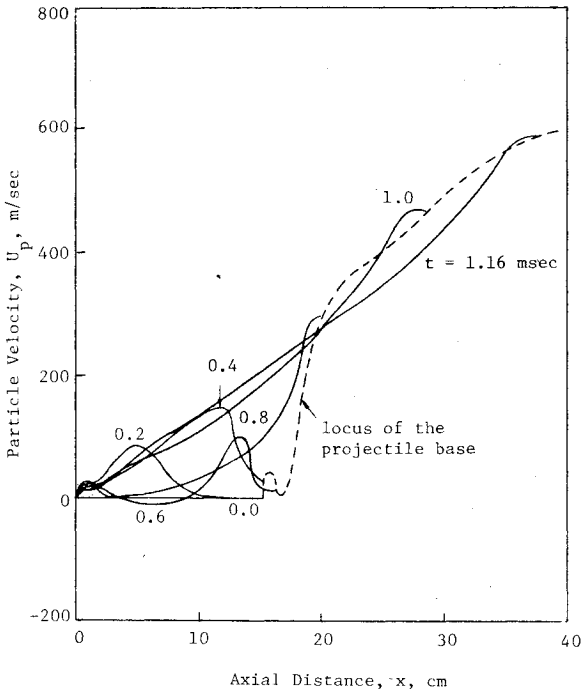

Fig. 6 Theoretically predicted particle velocity distributions at various times.

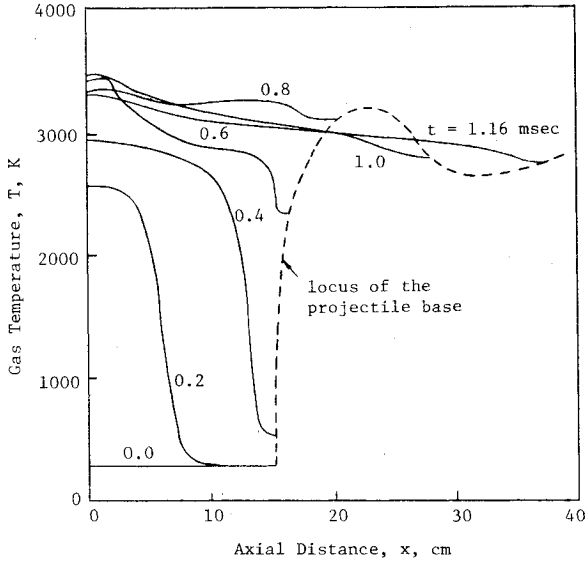

Fig. 7 Theoretically predicted gas temperature distributions at various times.

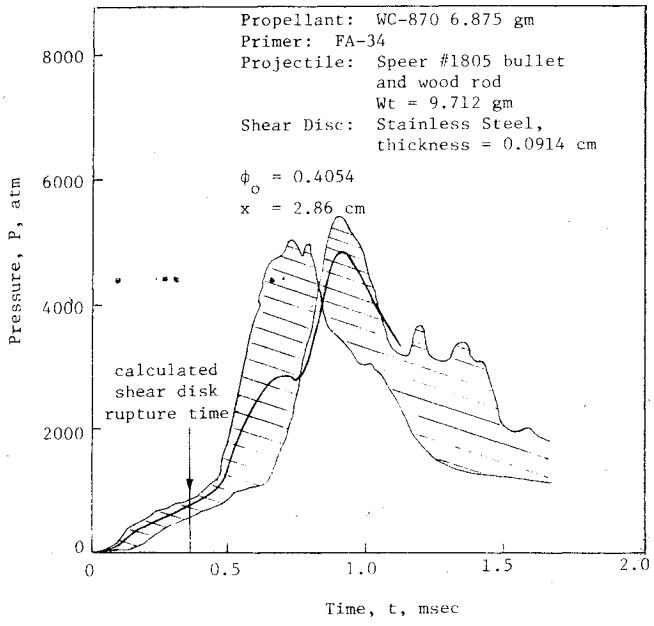

Fig. 8 Comparison of theoretically predicted pressure-time trace at $x=2.86$ cm with the composite pressure-time traces of three experimental test firings.

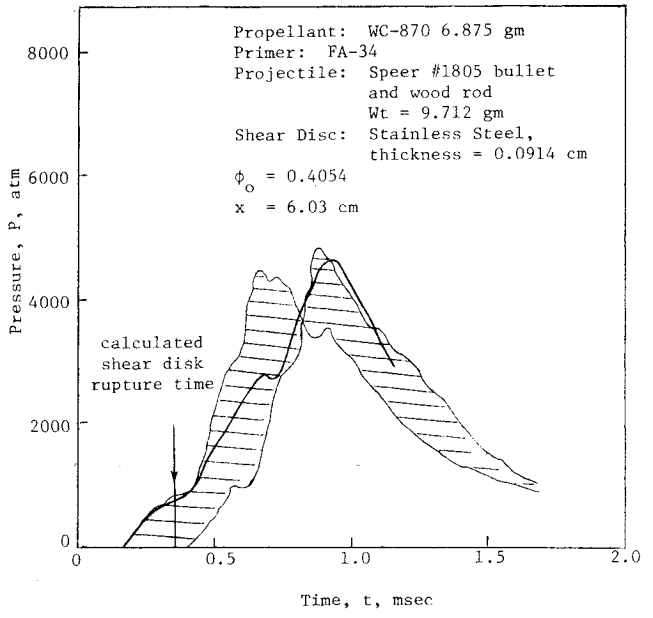

Fig. 9 Comparison of theoretically predicted pressure-time trace at $x=6.03$ cm with the composite pressure-time traces of three experimental test firings.

sealed with a stainless steel disk (0.0914 cm thick). A 30-caliber bullet (Speer #1805) was installed immediately in front of the shear disk. The total weight of the bullet and indicating wood rod was 9.712 g.

Figure 4 shows the theoretically predicted pressure distributions at various times. Owing to the compression wave resulting from the burning of granular propellants, the pressure distribution first develops a steep pressure gradient on its right-hand side. Then, a strong pressure gradient, caused by reflection of the compression wave from the projectile base, appears on the left-hand side of the peak, resulting in a reverse flow of gases from the downstream portion of the granular bed to the breech end. This reflection wave hits the breech end at $t \simeq 1$ ms. Finally, accompanied by projectile motion, the peak pressure decreases and the pressure in the fluidized bed becomes more uniform. The dashed curve shows the locus of the projectile base on the pressure distribution curve.

Figure 5 shows the theoretically predicted gas velocity distribution at various times. The primer blast causes an initial gas penetration into the granular bed near the breech end. Later, with combustion occurring in the granular bed, the peak of the gas velocity profile develops due to the steep pressure gradient and flow resistance in the bed. At 0.8 ms, flow reversal occurs as a result of strong adverse pressure gradient in the granular bed; it disappears as the granular bed expands further.

Figure 6 shows the theoretically predicted particle velocity distributions at various times. At the beginning of combustion, particle velocity is less than gas velocity because of the inertia of the particle and the tightly packed situation. At 0.6 ms, particle velocity becomes smaller and even negative in the middle portion of the bed. This is believed to be due to the complex effects of particle gasification, reflection of in-

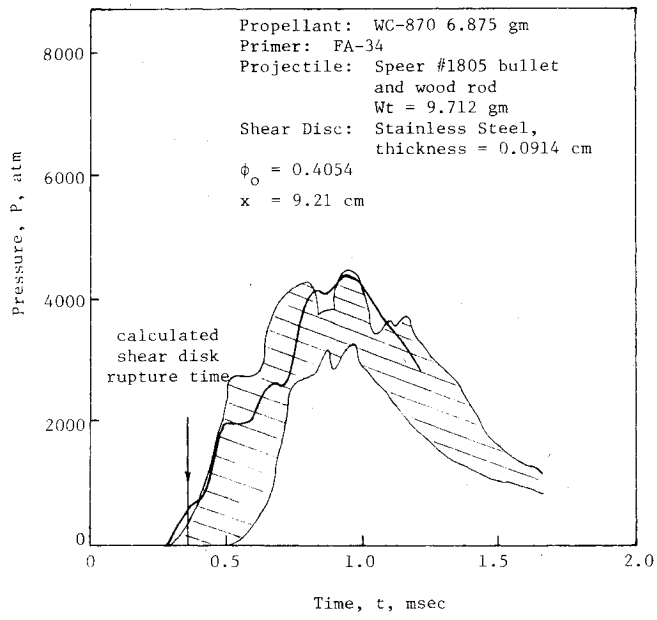

Fig. 10 Comparison of theoretically predicted pressure-time trace at $x=9.21$ cm with the composite pressure-time traces of three experimental test firings.

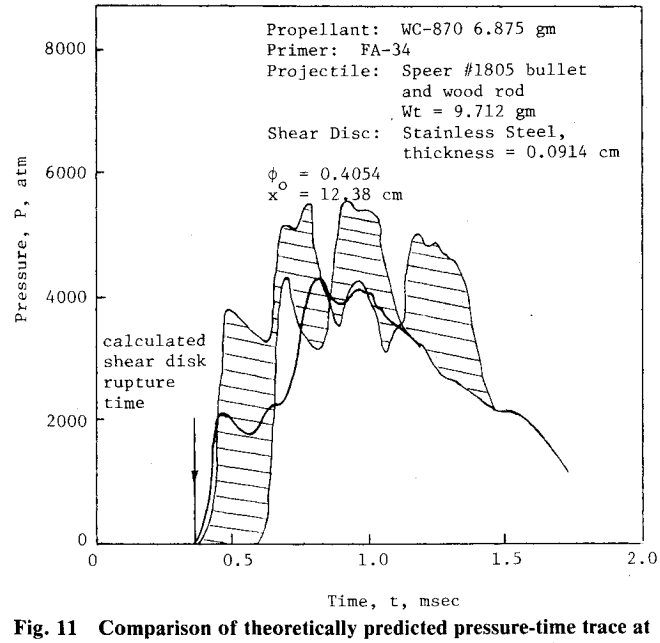

Fig. 11 Comparison of theoretically predicted pressure-time trace at $x=12.38$ cm with the composite pressure-time traces of three experimental test firings.

tragranular stress wave from the projectile base, and gas motion.[11] Later, as combustion occurs in the granular bed, the particle becomes smaller and fluidized; it can be entrained by the gas motion, and therefore moves faster.

Figure 7 shows the theoretically predicted temperature distributions at various times. Temperature gradients associated with gas penetration motion are salient in the beginning of the flame spreading and combustion processes. Following ignition along the entire length of the granular bed, the temperature distribution remains nearly uniform at various times.

Theoretically predicted pressure-time traces at various locations along the granular bed were superimposed on experimental data for three separate test firings, (see Figs. 8-11). The test firings were conducted under the same initial conditions mentioned earlier. Shaded regions in the figures represent composed *P-t* traces of the three test firings. Solid lines represent the theoretically calculated *P-t* traces. The comparison is made by superimposing the first discernible pressure rise time (at the nearest gage location to the primer) with the time required for the calculated pressure to rise noticeably. Based upon the direct comparison, the following observations can be made:

1) Predicted peak pressures at various axial locations are in good agreement with measured values.

2) Similar to the experimental measurements, calculated pressurization rates at downstream locations continue to rise, eventually overtaking upstream pressure traces.

3) After attaining peak pressures, predicted depressurization rates at different gage locations are generally consistent with experimental results.

4) Predicted times to reach peak pressures at all four gage locations are in reasonable agreement with experimental measurements; major portions of the predicted *P-t* traces lie in the shaded areas.

5) Rupture time of the shear disk for each firing, as measured by high-speed movie camera, is about the same as the first discernible pressure rise at the last pressure gage. This suggests that rupture of the shear disk is caused mainly by intragranular stress transmitted through the granular bed. Consistent with experimental measurements, the calculated force acting on the shear disk indicates that it is caused mainly by intragranular force.

Although the calculated results do not match perfectly with the experimental data of a particular test firing, the predicted results may differ less from that set of data than they do between separate experimental firings conducted at the same initial conditions. In general, good agreement between theoretical predictions and experimental data was obtained. This agreement supports the model MGBC developed at The Pennsylvania State University.

IV. Summary and Conclusions

1) In order to simulate the combustion processes of mobile granular propellants in a two-phase flow, boundary conditions must be adequately specified. Strong interaction and close coupling between boundary conditions and flow situations are noted. The form and total number of the boundary conditions depend upon the relative velocities of the gases and solid particles with respect to the solid boundary and the condition of fluidization.

2) Boundary conditions are obtained from physical conditions; extraneous boundary conditions are solved from a combined lumped-parameter analysis and the method of characteristics.

3) Calculated pressure-time traces from the mobile granular bed combustion (MGBC) code compare reasonably well with experimental data obtained from a simulated gun system.

4) In view of the agreement of the MGBC solution with the experimental data in this paper and with other granular bed compaction studies,[11] the MGBC code can be considered a useful tool for studying combustion processes in granular propellant beds. The code is helpful in explaining various combustion phenomena observed experimentally, and in studying the variation of physical parameters which cannot be easily measured.

Acknowledgment

This work represents a part of the results obtained from the research program performed under Grant No. DAAG 29-77-G-0163, sponsored by the Engineering Sciences Division of the U.S. Army Research Office at Research Triangle Park, North Carolina.

References

[1] Corner, J., *Theory of the Interior Ballistics of Guns*, John Wiley and Sons, Inc., New York, 1950.

[2]Kuo, K. K., Vichnevetsky, R. and Summerfield, M., "Theory of Flame Front Propagation in Porous Propellant Charges Under Confinement," *AIAA Journal*, Vol. 11, April 1973, pp. 444-451.

[3]Kuo, K. K., Koo, J. H., Davis, T. R., and Coates, G. R., "Transient Combustion in Mobile Gas-Permeable Propellants," *Acta Astronautica*, Vol. 3, July 1976, pp. 573-591.

[4]Krier, H. and Rajan, S., "Flame Spreading and Combustion in Packed Beds of Propellant Grains," AIAA Paper 75-240, AIAA 13th Aerospace Sciences Meeting, Jan. 1975.

[5]Gough, P. S., "The Flow of a Compressible Gas Through an Aggregate of Mobile Reacting Particles," Ph.D. Thesis, Dept. of Mechanical Engineering, McGill University, Dec. 1974.

[6]Fisher, E. B. and Trippe, A. P., "A Mathematical Model of Center Core Ignition in the 175 mm Gun," Calspan Rept. No. VQ-5163-D-2, March 1974.

[7]Kuo, K. K., "A Summary of the JANNAF Workshop on Theoretical Modeling and Experimental Measurements of the Combustion and Fluid Flow Processes in Gun Propellant Charges," 13th JANNAF Combustion Meeting, CPIA Pub. 281, Vol. 1, Dec. 1976, pp. 213-233.

[8]Chen, D. Y., "Transient Mobile Granular Bed Combustion of Solid Propellants with Moving Boundary," M.S. Thesis, Dept. of Mechanical Engineering, The Pennsylvania State University, Aug. 1979.

[9]Kuo, K. K., Yang, V., and Moore, B. B., "Intragranular Stress, Particle-Wall Friction and Speed of Sound in Granular Propellant Beds," *Journal of Ballistics*, Vol. 4, No. 1, 1980, pp. 697-730.

[10]Kuo, K. K., Moore, B. B., and Chen, D. Y., "Characterization of Mass Flow Rates for Various Percussion Primers," 7th International Colloquium on Gas-Dynamics of Explosions and Reactive Systems, Göttingen, West Germany, Aug. 1979; also in *AIAA Progress in Astronautics and Aeronautics—Gasdynamics of Detonations and Explosions*, Vol. 75, edited by J. R. Bowen, N. Manson, A. K. Oppenheim, and R. I. Soloukhin, New York, 1981.

[11]Yang, V., "Transient Granular Propellant Bed Compaction Caused by Mechanical and Gas Dynamic Methods," M.S. Thesis, Dept. of Mechanical Engineering, The Pennsylvania State University, Aug. 1980.

[12]Gough, P. S., "Computer Modeling of Interior Ballistics," U.S. Naval Ordnance Station Rept. IHCR 75-3, Oct. 15, 1975.

[13]Gough, P. S., "Numerical Analysis of a Two-Phase Flow with Explicit Internal Boundaries," NOS Rept. IHCR 77-5, April 1, 1977.

[14]Gough, P. S., "Two Dimensional Convective Flame Spreading in Packed Beds of Granular Propellant," Contract Rept. ARBRL-CR-00404, July 1979.

[15]Krier, H. and Kezerle, J. A., "A Separated Two-Phase Flow Analysis to Study Deflagration-to-Detonation Transition (DDT) in Granulated Propellant," *Seventeenth Symposium (International) on Combustion*, 1978, pp. 23-34.

[16]Davis, T. R. and Kuo, K. K., "Experimental Study of the Combustion Process in Granular Propellant Beds," *Journal of Spacecraft and Rockets*, Vol. 16, July-Aug. 1979, pp. 203-209.

[17]Koo, J. H. and Kuo, K. K., "Transient Combustion in Granular Propellant Beds. Part I: Theoretical Modeling and Numerical Solution of Transient Combustion Processes in Mobile Granular Propellant Beds," BRL Contract Rept. No. 346, Aug. 1977.

[18]Kuo, K. K. and Nydegger, C., "Flow Resistance Measurement and Correlation in a Packed Bed of WC-870 Ball Propellants," *Journal of Ballistics*, Vol. 2, No. 1, 1978, pp. 1-26.

[19]Andersson, K.E.B., "Pressure Drop in Ideal Fluidization," *Chemical Engineering Science*, Vol. 15, 1961, pp. 276-297.

[20]Denton, W. H., *General Discussion on Heat Transfer*, Institution of Mechanical Engineers and American Society of Mechanical Engineers, London, 1951, p. 370.

[21]Rowe, P. N. and Claxton, K. T., "Heat and Mass Transfer from a Single Sphere to Fluid Flowing Through an Array," *Transactions of the Institution of Chemical Engineers*, Vol. 43, 1965, pp. 321-331.

[22]Riefler, D. W. and Lowery, D. J., "Linear Burning Rates of Ball Propellants Based on Closed Bomb Firings," BRL Contract Rept. No. 172, Aug. 1974.